Nanoscopy of Living Brain Slices with Low Light Levels

Ilaria Testa,[1] Nicolai T. Urban,[1] Stefan Jakobs,[1] Christian Eggeling,[1] Katrin I. Willig,[1] and Stefan W. Hell[1,*]

[1]Department of NanoBiophotonics, Max Planck Institute for Biophysical Chemistry, Am Fassberg 11, 37077 Göttingen, Germany
*Correspondence: hell@nanoscopy.de
http://dx.doi.org/10.1016/j.neuron.2012.07.028

SUMMARY

Lens-based fluorescence microscopy, which has long been limited in resolution to about 200 nanometers by diffraction, is rapidly evolving into a nanoscale imaging technique. Here, we show that the superresolution fluorescence microscopy called RESOLFT enables comparatively fast and continuous imaging of sensitive, nanosized features in living brain tissue. Using low-intensity illumination to switch photochromic fluorescent proteins reversibly between a fluorescent and a nonfluorescent state, we increased the resolution more than 3-fold over that of confocal microscopy in all dimensions. Dendritic spines located 10–50 μm deep inside living organotypic hippocampal brain slices were recorded for hours without signs of degradation. Using a fast-switching protein increased the imaging speed 50-fold over reported RESOLFT schemes, which in turn enabled the recording of spontaneous and stimulated changes of dendritic actin filaments and spine morphology occurring on time scales from seconds to hours.

INTRODUCTION

Lens-based fluorescence microscopes, especially their confocal and two-photon variants (Denk et al., 1990), are unique in their ability to directly observe morphological changes and molecular interactions in living, functional brain tissue (Denk and Svoboda, 1997; Helmchen and Denk, 2005; Nägerl and Bonhoeffer, 2010; Nimchinsky et al., 2002; Yuste and Denk, 1995). Unfortunately, however, they are severely impaired by not being able to discern details closer together than about half of the wavelength of light (200–350 nm) due to diffraction (Abbe, 1873). The recent quest for light microscopy techniques providing subdiffraction resolution led to a powerful solution to this separation problem: by exploiting a mechanism for fluorescence inhibition, features that are closer together than the diffraction barrier are forced to emit sequentially so that they can be registered separately. This on-off principle of fluorescence emission (Hell, 2007, 2009) is most prominently harnessed in two distinct superresolution microscopy (nanoscopy) families: the coordinate-targeted

approach, encompassing the concepts called STED (Hell and Wichmann, 1994; Klar et al., 2000; Willig et al., 2006), RESOLFT (Hell, 2003, 2007, 2009; Hell et al., 2003, 2004; Schwentker et al., 2007), SSIM (Gustafsson, 2005; Heintzmann et al., 2002), etc., employs a patterned beam of light to precisely determine the coordinate range in the sample in which fluorophores are "on," i.e., allowed to emit. In contrast, in the stochastic approach, represented by PALM (Betzig et al., 2006), STORM (Huang et al., 2010; Rust et al., 2006), etc., the light intensity is adjusted to enable the emission of a single fluorophore randomly located within the 200–300 nm sized diffraction range. The coordinate is then precisely determined by projecting its fluorescence onto a grid detector, typically a camera.

A major benefit of the coordinate-targeted STED or RESOLFT approaches is their potential for fast imaging. This benefit originates from the fact that the coordinate of fluorescence emission is preset by the light pattern in use, which enables the grouping of signal of all fluorophores residing at the emission site. Thus, unlike the otherwise very powerful stochastic approaches, the coordinate-targeted methods do not require the serial on-off cycling and successive emission of hundreds of photons from individual fluorophores within the diffraction range. For these reasons, STED microscopy was successfully implemented for imaging dynamic structures in neurons, such as dendritic spines (Ding et al., 2009; Nägerl et al., 2008; Urban et al., 2011) and rapidly moving synaptic vesicles at video-rate (Westphal et al., 2008). But even though recent studies have shown STED to map spine dynamics both in cultured brain slices (Ding et al., 2009; Nägerl et al., 2008; Urban et al., 2011) and in vivo (Berning et al., 2012), the relatively high average laser power required for attaining substantial subdiffraction resolution, comparative to two-photon excitation microscopy, provide strong incentives for developing a coordinate-targeted approach for low-power operation (Hell, 2003, 2009; Hell et al., 2003, 2004; Hofmann et al., 2005; Schwentker et al., 2007). For if highly sensitive structures such as synapses are to be examined, if their subtle changes (Yuste and Bonhoeffer, 2001) and the corresponding causes (Kwon and Sabatini, 2011) are to be determined, then any potential disturbances of the structure and its physiological environment should be avoided. This is where the RESOLFT concept, proposed in 2003 (Hell, 2003; Hell et al., 2003, 2004), can provide a solution: as opposed to the stimulated emission employed by STED microscopy for modulating the fluorescence capability of fluorophores, RESOLFT microscopy (or nanoscopy) instead exploits long-lived dark and fluorescent states provided by reversibly photoswitchable fluorophores. Due to the long

lifetimes of the involved "on" and "off" states, the light intensities required for gaining equivalent subdiffraction resolution by RESOLFT are reduced by several orders of magnitude over STED (Dedecker et al., 2007; Hell, 2003; Hell et al., 2003, 2004; Hofmann et al., 2005; Schwentker et al., 2007).

A practical implementation of RESOLFT nanoscopy for imaging living cells and tissue samples with low light intensities has been demonstrated recently (Brakemann et al., 2011; Grotjohann et al., 2011) using two reversibly switchable fluorescent proteins (RSFPs), namely rsEGFP (Grotjohann et al., 2011) and Dreiklang (Brakemann et al., 2011). Both RSFPs are well suited for specific imaging tasks: rsEGFP exhibits extremely low switching fatigue, thus providing superresolution images repeatedly. The RSFP Dreiklang is switched on and off at wavelengths that are different from that required for fluorescent excitation, offering flexibility in image recording. A drawback of Dreiklang is that the light required for on-switching, 355 nm, lies in the more unfavorable ultraviolet spectrum. Both of these RESOLFT schemes were implemented in a confocalized point-scanning setup, which is particularly suitable for imaging scattering tissue. However, the images obtained in neuronal tissue were of low contrast and recorded near the surface of the tissue sample. In addition, they could not be taken fast enough to follow rapid dynamical processes. The RESOLFT scheme has also been implemented in a line-pattern scanning mode earlier (Schwentker et al., 2007) and also more recently (Rego et al., 2012), but the exposure times of many minutes per frame required in the latter recordings, limited its application to fixed cells. Thus, RESOLFT imaging (Brakemann et al., 2011; Grotjohann et al., 2011; Hofmann et al., 2005; Rego et al., 2012; Schwentker et al., 2007) has so far fallen short of the concept's real potential of imaging quickly and repeatedly living tissue at low levels of light. Our goal was to remedy these shortcomings and to improve the capabilities of superresolution fluorescence microscopy for imaging living neuronal tissue.

To achieve these ends, we built an RSFP-based RESOLFT microscope dedicated to subdiffraction 3D imaging (Jones et al., 2011; Klar et al., 2000) of dendritic spines inside living brain tissue, and optimized for use with a fast-switching variant of the ubiquitous RSFP Dronpa (Ando et al., 2004; Habuchi et al., 2005), specifically Dronpa-M159T (Stiel et al., 2007). Even though it has a slightly lower quantum yield than Dreiklang and rsEGFP, this RSFP was appealing due to its off-switching times of only about 0.4 ms, which should be contrasted to the off-switching times of 10–40 ms of rsEGFP and Dreiklang. On account of the high imaging contrast, we resolved fine details of individual spines within living hippocampal brain tissue. Moreover, we observed short-term variabilities of individual dendritic spines on the time scale of seconds, as well as long-term changes along larger stretches of spiny dendrites. The use of low light intensity levels permitted continuous image acquisition in three dimensions, hardly limited by bleaching, and absent of signs of light-induced damage or phototoxic stress. We demonstrate RESOLFT to be a highly expedient imaging technique for unraveling the morphology of intricate and delicate neuronal features, without further impairing or disturbing the physiological environment. Our results establish RESOLFT as a new paradigm for nanoscale imaging of living brain tissue.
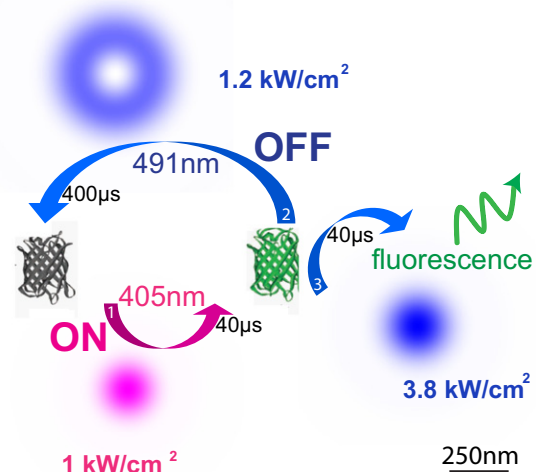

Figure 1. Wavelengths, Timing, and Focusing Scheme in a Point-Scanning RESOLFT Setup Employing Dronpa-M159T

(1) Fluorescent proteins are switched into the ON-state (purple arrow) using brief UV laser illumination with a Gaussian profile (wavelength λ = 405 nm, intensity $I_{ON} \approx$ 1 kW/cm^2, average power P_{avg} = 0.5 μW, exposure time t_{on} = 40 μs). (2) The molecules on the periphery are then switched off (large blue arrow) with a blue, doughnut-shaped beam (λ = 491 nm, $I_{OFF} \approx$ 1.2 kW/cm^2, P_{avg} = 3 μW, t_{OFF} = 400 μs). (3) The remaining molecules in the ON state are brought to fluoresce (small blue arrow) with a blue Gaussian-shaped beam (λ = 491 nm, $I_{EXC} \approx$ 3.8 kW/cm^2, P_{avg} = 3 μW, t_{EXC} = 40 μs). All power values in this manuscript are specified for the entrance pupil of the lens; the actual focal power is lower (by typically 20%), depending on the lens transmission at the particular wavelength. Focal intensity patterns of the individual beams are shown to scale, displayed next to the corresponding switching arrow. See also Figure S1.

RESULTS

RESOLFT Nanoscopy Setup

We constructed a RESOLFT nanoscope featuring dichroic mirrors and filters (see Figure S2 available online) dedicated for use with the green RSFP Dronpa-M159T and optimized for imaging convoluted structures inside neuronal tissue. The concept was implemented as a single point-scanning confocal microscope with three separate beams, each dedicated to one switching step of the fluorescent protein, overlapping in the focal region of the lens. The RSFPs were switched on using a nearly diffraction-limited circular light spot of 405 nm wavelength, switched off with a doughnut-shaped counterpart of 491 nm wavelength featuring a central intensity zero, and excited with another circular spot of light, also of 491 nm wavelength (Figure 1). When imaging, the application of these beams were cycled pixel by pixel, each with dwell times chosen according to the photo-switching kinetics of Dronpa-M159T (Figure S1). Whereas previous RESOLFT implementations required 10–20 ms for each beam-cycling step, this dwell time was here reduced to 400 μs, speeding up overall imaging more than 50-fold. Deep tissue imaging was facilitated by applying a glycerol-immersion lens (63×, Leica Microsystems, Wetzlar,

Germany) of 1.3 numerical aperture featuring a rotating collar for correcting spherical aberrations (Urban et al., 2011). Thus, we imaged neuronal structures between 5–50 μm deep beneath the surface of the living brain slices (Figure S3).

Dendritic actin structures, as the dendritic spines themselves and the synapses they form, are convoluted in all three dimensions (Hotulainen and Hoogenraad, 2010). Resolving fine details thus will generally require subdiffraction resolution not only in the xy plane, but also along the optical (z) axis. Therefore, we added an additional 491 nm beam and passed it through a spatial phase mask modulating the beam's wavefront such that an off-switching z doughnut is created in the focal region (Klar et al., 2000) for enhancing the resolution along the z axis (Figure S2). The combined use of an (x,y) and z doughnut typically yielded a resolution of (65 ± 10) nm in the focal plane (x,y) and 110–150 nm along the z axis and allowed us to perform optical sectioning with 60 nm step sizes. The z doughnut could be added at will, depending on whether we required the enhanced z resolution.

Dendritic Spines with Nanoscopic Resolution

The fast RESOLFT recording facilitated subdiffraction imaging of tagged structures with differing mobility. Neurons in hippocampal mouse brain slices were transfected to express Dronpa-M159T, either targeted to the cytosol or binding to actin. The latter was accomplished using Lifeact (Riedl et al., 2008), a short 17 amino acid long peptide labeling filamentous and globular actin without interfering with cellular processes or disturbing the assembly of native actin filaments. The differing localization in the neurons was clearly apparent, as shown in Figure 2. The actin-bound label was concentrated in dendritic spine heads and necks, with the dendrite proper only dimly visible, presumably due to the globular actin diffusing in the cytosol (Figure 2A). Actin bundles were frequently observed, running from spines into the dendritic shaft and intermittently along the periphery of the dendrites. Conversely, the neurons transfected with cytosolic Dronpa-M159T displayed a mostly homogeneous distribution of fluorescence along the dendrite (Figure 2B), with smaller and less voluminous spines tending to be dimmer than larger ones.

The high concentration of F-actin in dendritic spines proved ideal for imaging actin structures inside spines labeled with Lifeact-Dronpa-M159T (Figure 2C). In particular, by employing 3D resolution improvement, actin bundles extending from the spine head or neck into the dendritic shaft could be examined (Figure 2D). Without subdiffraction 3D resolution it would have been difficult to prove that these actin bundles were enclosed within the interior of the dendritic shaft and not merely close above or below the imaged dendrite (Movie S1). Such actin cables could be observed frequently, extending sometimes in one, sometimes in both directions along the dendrite or simply jutting out into the shaft. The length and trajectory of these actin bundles varied considerably, from long and straight to tightly curved. In neurons transfected with the cytosolic label nothing resembling these actin cables could be observed (Figure 2E), but no matter which specific labeling was used, the 3-fold resolution enhancement in all three spatial dimensions greatly increased the level of detail with which the intricate morphology of the spine heads and necks could be observed (Movie S2).
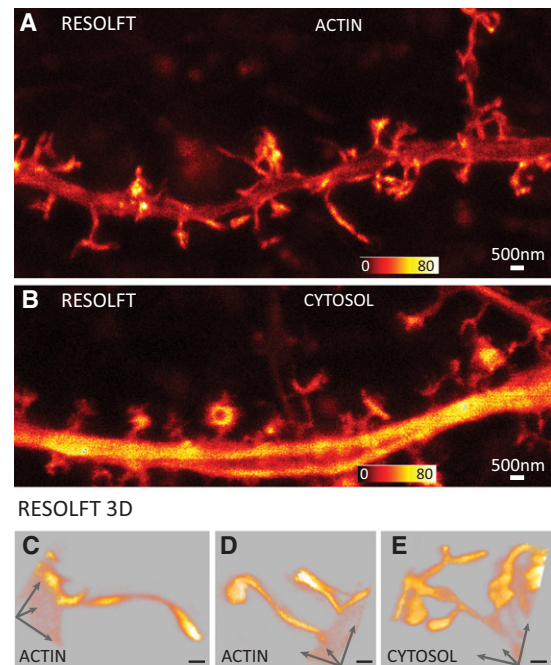

Figure 2. RESOLFT Nanoscopy of Living Neurons in Hippocampal Slices Recorded at Ultralow Light Levels

Superresolved RESOLFT images of dendrites of pyramidal neurons labeled with Dronpa-M159T binding to actin (A) and in the cytosol (B). The raw-data images are maximum intensity projections of multiple z planes, each 500 nm apart from each other along the optical axis. Multiple planes were recorded to incorporate the entire three-dimensional structure of the dendrite and its spines into the image.

(A) Field of view 10 × 20 μm², 5 planes, pixel size 25 nm, imaging duration 160 s; the dendrite was located 35 μm beneath the tissue surface.

(B) Field of view 7 × 20 μm², 3 planes, pixel size 30 nm, pixel dwell-time 500 μs, imaging duration 120 s; located 30 μm beneath the tissue surface. The three lower panels are 3D renditions of RESOLFT images with enhanced resolution in all spatial dimensions and depict dendritic spines with either the actin-fused (C and D) or cytosolic (E) labeling.

In (C) and (D) actin filaments can be seen to extend from the spine neck well into the dendritic shaft. The first panel (C) displays a field of view of 4.8 × 3 × 1.2 μm³, the second (D) of 4 × 6 x 1.2 μm³ and the third (E) of 4 x4 × 0.6 μm³. The voxel size is 40 × 40 × 60 nm³, pixel dwell time 500 μs. The spines were all located between 25 and 35 μm deep inside the slices. Scale bars = 500 nm. See also Figure S2 and Movies S1 and S2.

The superior resolution became even more evident when observing actin substructures within dendritic spine heads. A small number of spine heads showed distinct ring-like structures (Izeddin et al., 2011) —or holes—in the interior (Figure 3). Being of the order of the diffraction limit, these holes were not discernible in the confocal counterpart images. Furthermore, we discerned spine necks with nonuniform thickness, either tapering or widening toward the spine head, exhibiting distinct bulges or protrusions along their length, or featuring substantially dimmer stretches along otherwise homogeneous spine necks.

Continuous Time-Lapse Imaging

The fast imaging speed and minimal illumination intensities inherent to this RESOLFT microscopy implementation were ideally
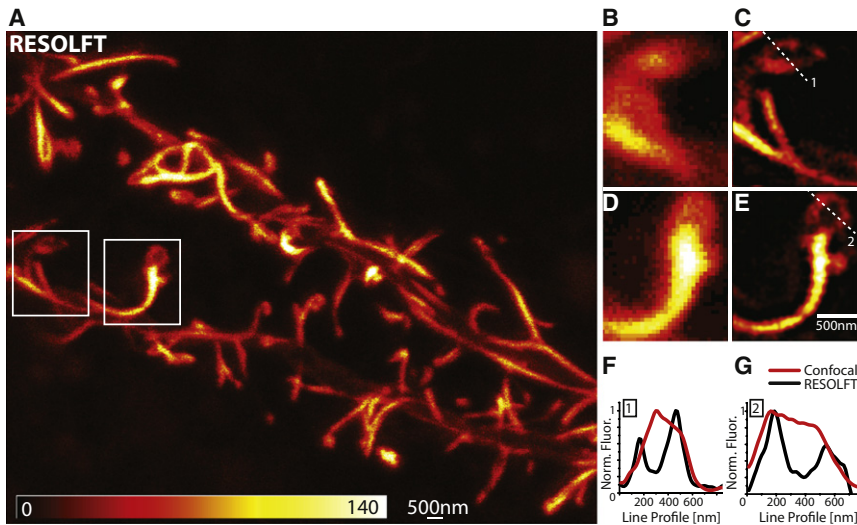
Figure 3. RESOLFT Nanoscopy Reveals Actin Distribution within Dendritic Spines

(A) Dendrites labeled with Lifeact-Dronpa-M159T display concentrations of actin within dendritic spines. The dendrites were located in the second to third cell layer of the brain slice, 38 μm beneath the tissue surface (see also Figure S3). Actin substructures within spine heads (see boxed areas) are resolved in nanoscopic detail by RESOLFT (A, C, and E), but not in the diffraction-limited confocal mode (B and D). The data in (C) and (E) was deconvolved with a nonlinear algorithm using the effective point-spread-function of the imaging modality, a Gaussian function of 70 nm full-width-half-maximum. All other images show raw data.

(F, and G) The gain in resolution is evident when comparing intensity profiles taken along lines 1 and 2 (indicated in C and E) in both the confocal deconvolved (red lines) and RESOLFT deconvolved data (black lines). All images are maximum intensity projections of multiple z planes.

suited to observe dynamic processes and movements taking place on time scales from seconds to hours (Engert and Bonhoeffer, 1999; Matus, 2000). At first, images were recorded while maintaining the slices at room temperature. Time-lapse recordings were taken continuously over several hours, scrutinizing for any signs of movement, morphological changes, or photodamage. To ensure that any observed dynamics were not simply an artifact caused by random defocus, we routinely recorded 3–5 optical sections of each imaged area and combined them into a maximum intensity projection. But despite exposing stretches of dendrites to constant laser illumination, the observed structures were stable and mostly static. Typical signs of phototoxic effects, such as dendrite blebbing or rapid, intense bleaching, were not observed.

Next, the sample chamber and the objective lens were heated to 35°C, and individual stretches of dendrites were observed in time-lapse imaging series. Spontaneous morphological changes of dendritic spines were observed more frequently, if still rarely, as well as individual spine movement or the shifting of entire regions of the dendrite. To observe processes taking place at various speeds, we alternated between two different imaging schemes: fast scans of small areas, usually containing one or more dendritic spines, complemented with larger area scans comprising an overview over longer stretches of dendrites. In Figure 4A we imaged a dendrite repeatedly over a period of three hours. During this time we recorded several large overview images (11.5 × 8 μm²) to observe the overall behavior of the dendrite, interspersed with several series of small (4.2 × 3 μm²), fast scans (40 frames at 7 s / frame) to catch any fast dynamical processes. Over the 3 hr course of the observation (Figure 4A, left and right) small but distinct morphological changes took place over minutes to hours, such as individual spines drifting in and out of focus and moving in space. When comparing closer time frames (Figure 4A, center) only minor changes seem to occur. Interestingly, observed on a much shorter time scale (seconds), the spines can be seen to be in constant movement (Movie S3). Note, that between the first and the last frame of each 40-frame

imaging series, there was less than 10% decrease in fluorescence signal in the specific region (see also Figures S4A and S4B).

The imaging speed of the microscope was fast enough to image individual spines in subsecond intervals. For test purposes, we recorded individual frames (1.75 × 0.9 μm²), each lasting only 0.75 s (Figure S4). In between each frame we shifted the sample slightly along the x axis, so that a single dendritic spine progressed through the series of frames, showing that sub-second dynamic processes could be recorded with RESOLFT.

To test the capability of long-term imaging, and to elucidate any possible effects of the illumination on the sensitive neuronal tissue, we imaged stretches of dendrites continuously for several hours, thereby exposing these areas to constant cycling illumination (Figure 4B). Over the course of minutes to hours, gradual movements and morphological changes of spines and dendrites were observed, with no apparent correlation between irradiation time and observed movement. At the end of the measurements, no signs of phototoxic stress or photodamage were observed, and the bleaching of the irradiated dendrite was negligible (see also Movie S4).

During all these time-lapse experiments, we scrutinized for typical signs of photodamage, such as blebbing of the dendrite, rapid and severe bleaching or dimming, strong feature drift, irregular changes of spines, inhomogenities along individual dendrites or sudden increase in tissue opacity. Furthermore, we watched closely for any sudden deviations in the frequency or magnitude of the dynamic processes. None of these phenomena were noted.

Observation of Stimulated Morphological Changes

As further assessment toward the aptitude of our RESOLFT microscope for long-term imaging, we examined induced morphological changes of dendritic spines following chemical stimulation. To this end, we exposed hippocampal slices to a bath solution containing tetraethylammonium chloride (TEA-Cl), a potassium channel blocker, so as to induce morphological
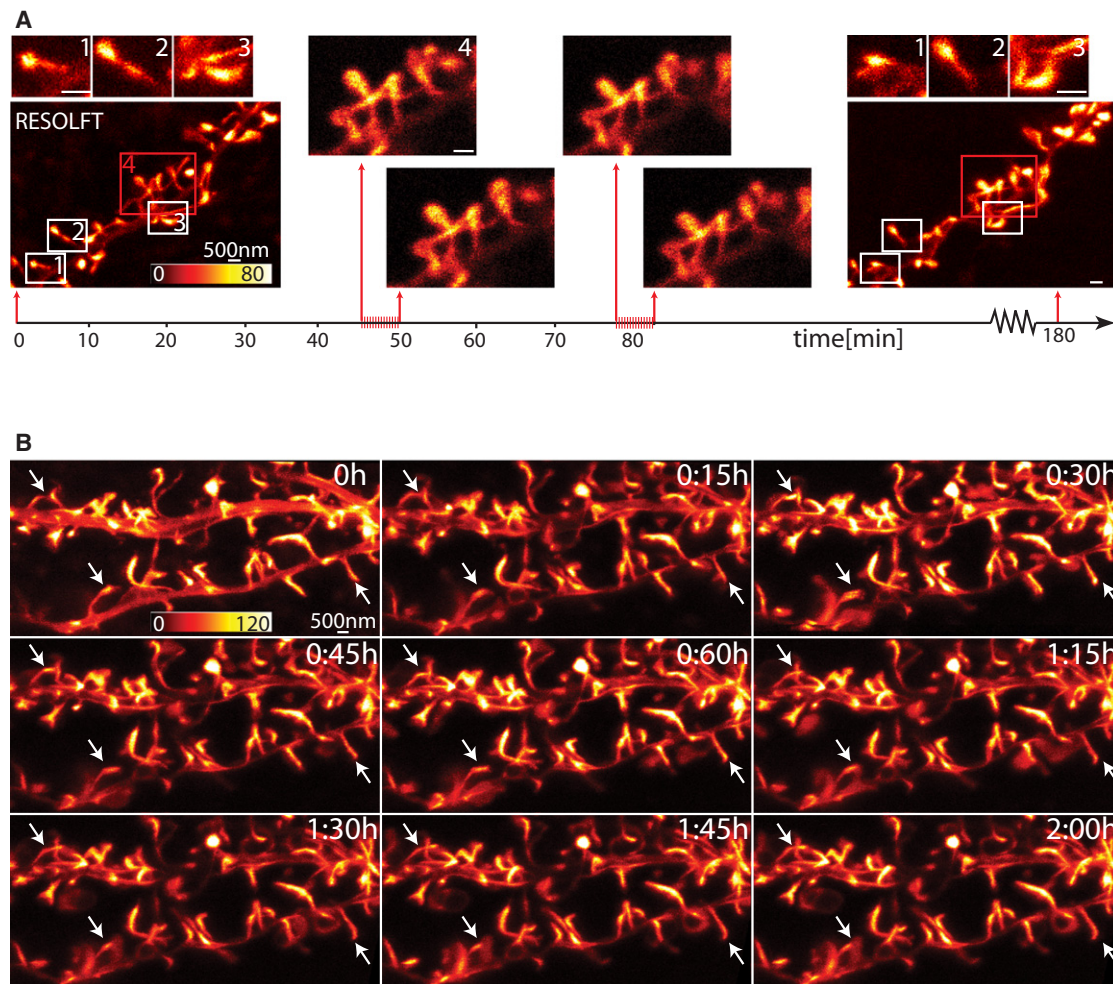
Figure 4. Continuous Time-Lapse Imaging with RESOLFT Reveals Spontaneous Rearrangements of Actin-Labeled Dendritic Spines on Short- and Long-Term Time Scales

The ultralow light levels inherent in RESOLFT microscopy facilitate continuous imaging of dendrites and individual spines. Spontaneous actin dynamics on different time scales, from seconds to hours, can be observed in real-time.

(A) A dendrite from a Lifeact-Dronpa-M159T labeled neuron was imaged continuously with RESOLFT over several hours, revealing slight changes and movements of individual spines (boxed areas 1, 2, and 3). At several intervals during the experiment, we recorded series of fast, consecutive images (7 s/frame), consisting of 40 frames each (boxed area 4). Slight spine movements were observed during these short time windows (see also Movie S3).

(B) Extensive spontaneous movement and morphological changes of entire dendritic stretches were observed by continual recording of 45 image frames over a period of several hours without incurring visible photodamage (see also Movie S4). The dendrite was labeled with Lifeact-Dronpa-M159T.

The overview images are maximum intensity projections of multiple z-planes; the 40-frame image series in (A) show single z planes. All images show raw data. Scale bars 500 nm. See also Figure S4.

changes in synapses according to a chemical long-term potentiation (LTP) protocol (Arellano et al., 2007; Hosokawa et al., 1995). Images were recorded before, during, and after bath application of the LTP-medium (Figure 5). We generally observed changes of spine head shape and size, as well as neck length and width within 5–30 min after application of the LTP medium (Figure 5B). Following the LTP stimulation, the spine necks widened overall (on average by 39%, from 143 ± 5 nm to 194 ± 6 nm, mean $\pm$ SEM, n = 24; $p \ll 0.001$, paired t test) and shortened slightly (on average by 7%, from 1.2 ± 0.2 μm to 0.9 ± 0.2 μm, n = 24; $p < 0.008$, paired t test). The cross-section of the spine heads exhibited strong bidirectional fluctuation with

an average increase similar to the changes in spine neck width (on average 35%, from 0.21 ± 0.04 μm^2 to 0.22 ± 0.03 μm^2, n = 24); this did not significantly alter the overall mean value across the population, however (n = 24, p = 0.62, paired t test; Figure S5). After this period of fluctuation the dynamic alterations mostly stopped and the induced morphological changes were maintained over the further course of the experiment, even when observed for several more hours (Figure 5). In contrast to the abrupt, triggered changes induced by the chemical LTP, we did not observe any correlation between irradiation time and frequency or magnitude of morphological changes and movement.
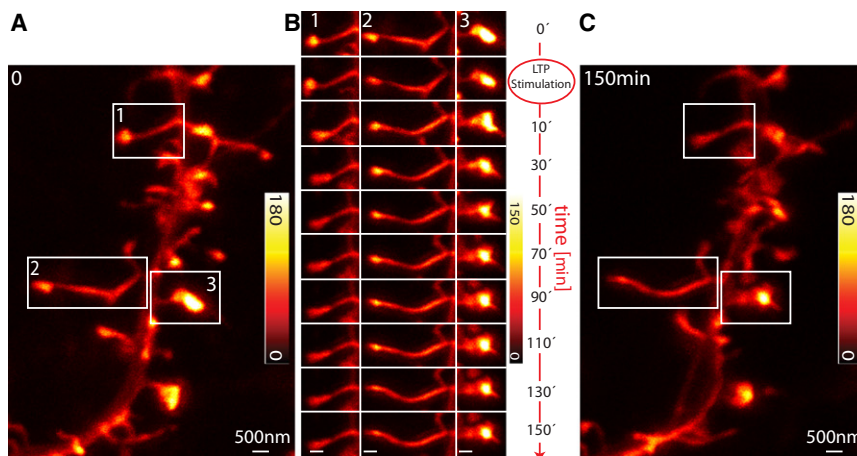
Figure 5. Morphological Changes of Dendritic Spines Induced by Chemical LTP Stimulation

A spiny dendrite of a Lifeact-Dronpa-M159T labeled CA1 pyramidal neuron before (A) and after (C) chemical LTP stimulation. The morphology of three individual spines (boxed areas 1, 2, and 3) can be observed over the time course of 2.5 hr (B)—before, during, and at subsequent intervals after chemical LTP stimulation. Clear morphological changes occurred during and up to 30 min following stimulation (see also Figure S5). After that the spines are more or less static, despite continuous irradiation for more than two hours. All images show raw data and are maximum intensity projections of several z planes.

DISCUSSION

Since structural and functional studies of synapses call for observation of nanosized, highly sensitive features, the future of neuroscience will rely heavily on lens-based superresolution optical microscopy (Dani et al., 2010; Nägerl et al., 2008; Urban et al., 2011). Our study has shown that the RESOLFT superresolution concept has a, so far, unique potential to image living neuronal tissue sustainably over long time periods. The demonstrated imaging speed and 3D resolution enabled us to track actin dynamics in dendritic spines and the overall spine morphology for several hours by continuous observation, both after chemical stimulation and under natural conditions. The switching capability and speed of the RSFP Dronpa-M159T facilitated the observation of both fast dynamical processes occurring within seconds, as well as more gradual long-term changes. Specific regions could be imaged over and over again, recording well over 100 superresolved frames with minimal photobleaching and photodamage.

The observed movements and morphological changes of dendritic spines correspond well with previous experiments using STED microscopy in brain slices and in vivo mouse brains (Berning et al., 2012), in regard to appearance and overall magnitude. These STED recordings used subnanosecond pulsed illumination with 25–30 mW average power (Urban et al., 2011), which should be compared with the average powers of 0.5–3 μW of continuous wave illumination used in our RESOLFT scheme. This seems to vindicate the use of these techniques in observing sensitive neuronal structures such as synapses over long time periods. We can only speculate, however, as to any putative dependence of the frequency of dynamic events on the irradiation time or on the light intensity implemented in these experiments. The radical change in employed power and wavelength connected with the use of a different on-off switching mechanism offers a unique opportunity, however, to compare possible influences of different light microscopy techniques and light intensities on neuronal dynamics. In any case, the low light levels required for overcoming the diffraction barrier when using the RESOLFT scheme offers hitherto unachieved safety buffers. Further augmentations of living tissue compatibility

can be expected by shifting the illumination toward the redder spectral region for use with prospective photoswitchable proteins in the red wavelength regime. The use of red illumination would concomitantly reduce scattering inside brain tissue, thus allowing even deeper tissue imaging.

Since RESOLFT is readily implemented with confocal detection as shown, our observations are not limited to the upper layer of the sample but can penetrate for several cell layers inside hippocampal brain slices. The penetration depth can be substantially increased by implementing more sophisticated aberration correction schemes, such as active wavefront modification (Booth et al., 2002), or by resorting to multiphoton absorption for switching and fluorescence generation.

A caveat of deep tissue imaging, namely that ever-increasing power levels are required to penetrate further into the tissue, should not present practical restrictions to RESOLFT microscopy due to the low light levels inherent in this technique. By the same token, superresolution RESOLFT microscopy should be readily applicable to in vivo imaging of the living brain, as has already been demonstrated for STED (Berning et al., 2012). In light of the even superior compatibility of RESOLFT microscopy with live-cell conditions, our results open an arguably unexpected door to imaging neuronal function of living brains in vivo, e.g., of a living mouse, with highest resolution and negligible perturbations. Altogether, our results clearly demonstrate a new paradigm to imaging of living neuronal tissue on the nanoscale.

EXPERIMENTAL PROCEDURES

RESOLFT Microscope

Our home-built 3D RESOLFT microscope was implemented with a glycerol objective lens having a correction collar. The microscope utilized four separate beam paths for generating coaligned focal light spots: three at 491 nm wavelength for excitation and OFF switching and one at 405 nm for ON switching of the fluorophores (Figure 1). The three focal spots at 491 nm comprised (1) a normal diffraction-limited focal spot with a nearly Gaussian profile for reading out the fluorescence signal, (2) a focal intensity distribution with a central minimum ("zero") for OFF switching at the focal periphery in the xy plane, obtained by a passing the beam through a vortex phase mask (463 nm mask, vortex plate VPP-A, RPC Photonics, Rochester, NY), (3) a focal intensity

distribution with a central minimum ("zero") for OFF switching at the focal periphery along the optical (z) axis, obtained by passing the beam through a home-built 0–π phase mask. The first two focal intensity spots were both generated by the same laser diode (Calypso 50, Cobolt, Stockholm, Sweden). The third focal spot was generated using an identical, but separate, laser diode (Calypso 50, Cobolt), to avoid interference effects in the focal volume. The fourth focal spot, again with a normal diffraction-limited Gaussian profile, was generated by a laser diode at 405 nm wavelength (BCL-030-405-S, CrystaLaser, Reno, NV) and used for the ON switching of the fluorescent protein (Figure S2).

Two separate objective lenses were used alternatively in this setup: an oil-immersion objective lens (HCX PC APO, 100 × , 1.4NA, oil; Leica Microsystems, Wetzlar, Germany) was used only for experiments shown in Figure 5 in which case neuronal features within 10 μm of the tissue surface were imaged. In general, a glycerol-immersion objective lens (PL APO, CORR CS, 63×, 1.3 NA, glycerol; Leica Microsystems) was used in order to penetrate deep enough into the tissue sample. Using this lens, we imaged Dronpa-M159T-labeled neurons between 10–50 μm deep inside the brain slices. The correction collar of the glycerol objective lens was adjusted for each specific imaging depth by maximizing the fluorescence signal—a result from minimizing the extent of the point spread function along the optical (z) axis.

A piezo system (ENV40/20, Piezosystem Jena, Jena, Germany) was used to move the objective lens along the optic axis in a range of 120 μm. A separate piezo stage (NV40, Piezosystem Jena) was implemented to translate the sample with nanometer precision in the xy plane. The fluorescence signal was filtered by a band-pass filter (532/70 nm) and detected by an avalanche photo diode (Perkin Elmer, Waltham, MA); fluorescence photons were only allowed to be counted when the 491 nm readout beam was switched on. The individual laser beam paths were triggered either by an acousto-optic modulator (MTS 130A3, Pegasus Optik GmbH, Wallenhorst, Germany) or by an acousto-optic tunable filter (AOTF.nC/TN, Pegasus Optik GmbH). The pulse sequence and duration were defined by a pulse generator (Model 9514, QUANTUM COMPOSERS, Bozeman, MT) and triggered by a fast acquisition card (MCA-3 Series/P7882, FAST ComTec GmbH, Oberhaching, Germany) pixel by pixel.

Organotypic Hippocampal Slice Cultures, Transfection, and Labeling

Hippocampal brain slices were prepared by dissecting hippocampi from postnatal day 5–7 wild-type C57BL/6 mice, which were then sectioned in 400 μm thick slices and embedded in a plasma clot on 0.14 mm thick glass coverslips. The slices were maintained in a roller incubator at 35°C in medium containing (in ml): BME 97, HBSS 50, horse serum 50, glucose (45%) 2, glutamine (200 mM) 1—according to the method of Gähwiler et al. (1997). Slice cultures were left to mature for 12 days in the incubator and were used in the experiments up to an age of 45 days in vitro after preparation.

For transfection, a modified Semliki Forest Virus was produced based on a pSCA3 vector (DiCiommo and Bremner, 1998). To create the actin-binding Lifeact label (Riedl et al., 2008), the coding sequence for Lifeact-Dronpa-M159T$^{v2.0}$ or alternatively Lifeact-Dronpa-M159T-GE was inserted into pSCA3; for the cytosolic label Dronpa-M159T$^{v2.0}$ was inserted instead. The variant Dronpa-M159T-GE is a modification of Dronpa-M159T (Stiel et al., 2007) containing altered N and C termini, and the variant Dronpa-M159T$^{v2.0}$ has an additional point mutation E218G (Willig et al., 2011). We did not observe a difference between neurons transfected with Lifeact-Dronpa-M159T$^{v2.0}$ and Lifeact-Dronpa-M159T-GE and therefore do not distinguish between these two labels in the manuscript. We injected the virus containing the nucleotid sequence for Lifeact-DronpaM159T or DronpaM159T into the CA1 and CA3 regions of the slice cultures using a patch pipette connected to a pressure generator (Tooheyspritzer, Toohey Company, Fairfield, NJ). The cultures were then incubated for at least 12 hr and imaged within 12–48 hr after transfection. For imaging, brain slices were transferred to an imaging chamber and maintained in artificial cerebrospinal fluid (ACSF) containing (in mM) NaCl 126, KCl 2.5, CaCl$_2$ 2.5, MgCl$_2$ 1.3, glucose 30 and HEPES 27; the pH was adjusted with NaOH to 7.4. The imaging chamber and the objective lens were generally heated to 35°C during the experiments.

LTP Stimulation and Experimental Timeline

Brain slices were imaged at multiple locations at the start of each experiment to ensure overall slice health and to acquire superresolved images of neurons in an unstimulated state for later reference. Prior to stimulation, a specific area was imaged repeatedly for a baseline period (typically acquiring up to three time points). To commence the chemical stimulation the regular ACSF was replaced with modified ACSF, designed to induce chemical long-term potentiation (LTP), containing (in mM): NaCl 99, KCl 5, CaCl$_2$ 5, MgCl$_2$ 0.1, glucose 20, HEPES 27, and TEA-Cl 25; pH was adjusted with NaOH to 7.4. After 10 min, the modified ACSF was washed out and the slice was suffused with regular ACSF. One image was typically recorded during stimulation and multiple frames following after stimulation. The duration and frequency of these recordings depended, among others, on the field of view and the number of optical sections acquired.

Image Acquisition and Analysis

Image acquisition was performed with the software IMSpector (www.imspector.de). Each image was recorded by applying a specific pulse scheme, pixel by pixel (Figure 1). The laser intensity used in our illumination scheme ranged between 1–10 kW/cm^2. The pixel dwell time was adjusted according to the illumination intensity and ranged between 300–1000 μs. The optical sectioning performed in the experiments varied, depending on whether the xy phase mask was used in combination with the z phase mask or by itself. If the xy phase mask was used alone, the optical sectioning along the z axis was performed in 500 nm steps. When the xy and z phase masks were used in tandem, the optical sectioning was performed in 60 nm steps. 3D image reconstruction was performed with the software AMIRA (Visage Imaging GmbH, Berlin, Germany). A linear deconvolution algorithm was used on the 3D reconstructions in Figure 2C and the images in Figures 3C and 3E. Movie S3 was deconvolved using 5 iterations of a Richardson-Lucy algorithm. All power values are specified for the entrance pupil of the lens; the actual focal power is lower (by typically 20%), depending on the lens transmission at the particular wavelength.

SUPPLEMENTAL INFORMATION

Supplemental Information includes five figures, four movies, and Supplemental Text and can be found with this article online at http://dx.doi.org/10.1016/j.neuron.2012.07.028.

REFERENCES

Abbe, E. (1873). Beiträge zur Theorie des Mikroskops und der mikroskopischen Wahrnehmung. Archiv für Mikroskopische Anatomie *9*, 413–468.

Ando, R., Mizuno, H., and Miyawaki, A. (2004). Regulated fast nucleocytoplasmic shuttling observed by reversible protein highlighting. Science *306*, 1370–1373.

Arellano, J.I., Espinosa, A., Fairén, A., Yuste, R., and DeFelipe, J. (2007). Non-synaptic dendritic spines in neocortex. Neuroscience *145*, 464–469.

Berning, S., Willig, K.I., Steffens, H., Dibaj, P., and Hell, S.W. (2012). Nanoscopy in a living mouse brain. Science *335*, 551.

Betzig, E., Patterson, G.H., Sougrat, R., Lindwasser, O.W., Olenych, S., Bonifacino, J.S., Davidson, M.W., Lippincott-Schwartz, J., and Hess, H.F. (2006). Imaging intracellular fluorescent proteins at nanometer resolution. Science *313*, 1642–1645.

Booth, M.J., Neil, M.A.A., Juskaitis, R., and Wilson, T. (2002). Adaptive aberration correction in a confocal microscope. Proc. Natl. Acad. Sci. USA *99*, 5788–5792.

Brakemann, T., Stiel, A.C., Weber, G., Andresen, M., Testa, I., Grotjohann, T., Leutenegger, M., Plessmann, U., Urlaub, H., Eggeling, C., et al. (2011). A reversibly photoswitchable GFP-like protein with fluorescence excitation decoupled from switching. Nat. Biotechnol. *29*, 942–947.

Dani, A., Huang, B., Bergan, J., Dulac, C., and Zhuang, X. (2010). Superresolution imaging of chemical synapses in the brain. Neuron *68*, 843–856.

Dedecker, P., Hotta, J.I., Flors, C., Sliwa, M., Uji-i, H., Roeffaers, M.B.J., Ando, R., Mizuno, H., Miyawaki, A., and Hofkens, J. (2007). Subdiffraction imaging through the selective donut-mode depletion of thermally stable photoswitchable fluorophores: numerical analysis and application to the fluorescent protein Dronpa. J. Am. Chem. Soc. *129*, 16132–16141.

Denk, W., and Svoboda, K. (1997). Photon upmanship: why multiphoton imaging is more than a gimmick. Neuron *18*, 351–357.

Denk, W., Strickler, J.H., and Webb, W.W. (1990). Two-photon laser scanning fluorescence microscopy. Science *248*, 73–76.

DiCiommo, D.P., and Bremner, R. (1998). Rapid, high level protein production using DNA-based Semliki Forest virus vectors. J. Biol. Chem. *273*, 18060–18066.

Ding, J.B., Takasaki, K.T., and Sabatini, B.L. (2009). Supraresolution imaging in brain slices using stimulated-emission depletion two-photon laser scanning microscopy. Neuron *63*, 429–437.

Engert, F., and Bonhoeffer, T. (1999). Dendritic spine changes associated with hippocampal long-term synaptic plasticity. Nature *399*, 66–70.

Gähwiler, B.H., Capogna, M., Debanne, D., McKinney, R.A., and Thompson, S.M. (1997). Organotypic slice cultures: a technique has come of age. Trends Neurosci. *20*, 471–477.

Grotjohann, T., Testa, I., Leutenegger, M., Bock, H., Urban, N.T., Lavoie-Cardinal, F., Willig, K.I., Eggeling, C., Jakobs, S., and Hell, S.W. (2011). Diffraction-unlimited all-optical imaging and writing with a photochromic GFP. Nature *478*, 204–208.

Gustafsson, M.G.L. (2005). Nonlinear structured-illumination microscopy: wide-field fluorescence imaging with theoretically unlimited resolution. Proc. Natl. Acad. Sci. USA *102*, 13081–13086.

Habuchi, S., Ando, R., Dedecker, P., Verheijen, W., Mizuno, H., Miyawaki, A., and Hofkens, J. (2005). Reversible single-molecule photoswitching in the GFP-like fluorescent protein Dronpa. Proc. Natl. Acad. Sci. USA *102*, 9511–9516.

Heintzmann, R., Jovin, T.M., and Cremer, C. (2002). Saturated patterned excitation microscopy—a concept for optical resolution improvement. J. Opt. Soc. Am. A Opt. Image Sci. Vis. *19*, 1599–1609.

Hell, S.W. (2003). Toward fluorescence nanoscopy. Nat. Biotechnol. *21*, 1347–1355.

Hell, S.W. (2007). Far-field optical nanoscopy. Science *316*, 1153–1158.

Hell, S.W. (2009). Microscopy and its focal switch. Nat. Methods *6*, 24–32.

Hell, S.W., and Wichmann, J. (1994). Breaking the diffraction resolution limit by stimulated emission: stimulated-emission-depletion fluorescence microscopy. Opt. Lett. *19*, 780–782.

Hell, S.W., Jakobs, S., and Kastrup, L. (2003). Imaging and writing at the nanoscale with focused visible light through saturable optical transitions. Appl. Phys. A Mater. Sci. Process. *77*, 859–860.

Hell, S.W., Dyba, M., and Jakobs, S. (2004). Concepts for nanoscale resolution in fluorescence microscopy. Curr. Opin. Neurobiol. *14*, 599–609.

Helmchen, F., and Denk, W. (2005). Deep tissue two-photon microscopy. Nat. Methods *2*, 932–940.

Hofmann, M., Eggeling, C., Jakobs, S., and Hell, S.W. (2005). Breaking the diffraction barrier in fluorescence microscopy at low light intensities by using reversibly photoswitchable proteins. Proc. Natl. Acad. Sci. USA *102*, 17565–17569.

Hosokawa, T., Rusakov, D.A., Bliss, T.V., and Fine, A. (1995). Repeated confocal imaging of individual dendritic spines in the living hippocampal slice: evidence for changes in length and orientation associated with chemically induced LTP. J. Neurosci. *15*, 5560–5573.

Hotulainen, P., and Hoogenraad, C.C. (2010). Actin in dendritic spines: connecting dynamics to function. J. Cell Biol. *189*, 619–629.

Huang, B., Babcock, H., and Zhuang, X. (2010). Breaking the diffraction barrier: super-resolution imaging of cells. Cell *143*, 1047–1058.

Izeddin, I., Specht, C.G., Lelek, M., Darzacq, X., Triller, A., Zimmer, C., and Dahan, M. (2011). Super-resolution dynamic imaging of dendritic spines using a low-affinity photoconvertible actin probe. PLoS ONE *6*, e15611.

Jones, S.A., Shim, S.H., He, J., and Zhuang, X. (2011). Fast, three-dimensional super-resolution imaging of live cells. Nat. Methods *8*, 499–508.

Klar, T.A., Jakobs, S., Dyba, M., Egner, A., and Hell, S.W. (2000). Fluorescence microscopy with diffraction resolution barrier broken by stimulated emission. Proc. Natl. Acad. Sci. USA *97*, 8206–8210.

Kwon, H.B., and Sabatini, B.L. (2011). Glutamate induces de novo growth of functional spines in developing cortex. Nature *474*, 100–104.

Matus, A. (2000). Actin-based plasticity in dendritic spines. Science *290*, 754–758.

Nägerl, U.V., and Bonhoeffer, T. (2010). Imaging living synapses at the nanoscale by STED microscopy. J. Neurosci. *30*, 9341–9346.

Nägerl, U.V., Willig, K.I., Hein, B., Hell, S.W., and Bonhoeffer, T. (2008). Live-cell imaging of dendritic spines by STED microscopy. Proc. Natl. Acad. Sci. USA *105*, 18982–18987.

Nimchinsky, E.A., Sabatini, B.L., and Svoboda, K. (2002). Structure and function of dendritic spines. Annu. Rev. Physiol. *64*, 313–353.

Rego, E.H., Shao, L., Macklin, J.J., Winoto, L., Johansson, G.A., Kamps-Hughes, N., Davidson, M.W., and Gustafsson, M.G. (2012). Nonlinear structured-illumination microscopy with a photoswitchable protein reveals cellular structures at 50-nm resolution. Proc. Natl. Acad. Sci. USA *109*, E135–E143.

Riedl, J., Crevenna, A.H., Kessenbrock, K., Yu, J.H., Neukirchen, D., Bista, M., Bradke, F., Jenne, D., Holak, T.A., Werb, Z., et al. (2008). Lifeact: a versatile marker to visualize F-actin. Nat. Methods *5*, 605–607.

Rust, M.J., Bates, M., and Zhuang, X.W. (2006). Sub-diffraction-limit imaging by stochastic optical reconstruction microscopy (STORM). Nat. Methods *3*, 793–795.

Schwentker, M.A., Bock, H., Hofmann, M., Jakobs, S., Bewersdorf, J., Eggeling, C., and Hell, S.W. (2007). Wide-field subdiffraction RESOLFT microscopy using fluorescent protein photoswitching. Microsc. Res. Tech. *70*, 269–280.

Stiel, A.C., Trowitzsch, S., Weber, G., Andresen, M., Eggeling, C., Hell, S.W., Jakobs, S., and Wahl, M.C. (2007). 1.8 Å bright-state structure of the reversibly switchable fluorescent protein Dronpa guides the generation of fast switching variants. Biochem. J. *402*, 35–42.

Urban, N.T., Willig, K.I., Hell, S.W., and Nägerl, U.V. (2011). STED nanoscopy of actin dynamics in synapses deep inside living brain slices. Biophys. J. *101*, 1277–1284.

Westphal, V., Rizzoli, S.O., Lauterbach, M.A., Kamin, D., Jahn, R., and Hell, S.W. (2008). Video-rate far-field optical nanoscopy dissects synaptic vesicle movement. Science *320*, 246–249.

Willig, K.I., Rizzoli, S.O., Westphal, V., Jahn, R., and Hell, S.W. (2006). STED microscopy reveals that synaptotagmin remains clustered after synaptic vesicle exocytosis. Nature *440*, 935–939.

Willig, K.I., Stiel, A.C., Brakemann, T., Jakobs, S., and Hell, S.W. (2011). Dual-label STED nanoscopy of living cells using photochromism. Nano Lett. *11*, 3970–3973.

Yuste, R., and Bonhoeffer, T. (2001). Morphological changes in dendritic spines associated with long-term synaptic plasticity. Annu. Rev. Neurosci. *24*, 1071–1089.

Yuste, R., and Denk, W. (1995). Dendritic spines as basic functional units of neuronal integration. Nature *375*, 682–684.